

Electronic and vibrational properties of Pu_3M ($M = \text{Al, Ga, In, and Tl}$): A first-principles studyMenglei Li ¹, Yu Yang,^{2,*} Fawei Zheng,² Cong Wang,² and Ping Zhang^{2,3,4,5,6,†}¹*Department of Physics, Capital Normal University, Beijing 100048, China*²*LCP, Institute of Applied Physics and Computational Mathematics, Beijing 100088, China*³*Center for Fusion Energy Science and Technology, CAEP, Beijing 100084, China*⁴*Beijing Computational Science Research Center, Beijing 100084, China*⁵*Center for Applied Physics and Technology, Peking University, HEDPS, Beijing 100871, China*⁶*Compression Science Research Center, CAEP, Mianyang 621900, China*

(Received 27 June 2019; revised manuscript received 9 October 2019; published 1 November 2019)

We investigated the structural, electronic, magnetic, and phonon properties of Pu_3M , where $M = \text{Al, Ga, In, and Tl}$, using first-principles calculations with the spin-orbit coupling taken into consideration. All four compounds are found to contain transverse phonons along [011] and [111] that remarkably soften at the boundaries of the first Brillouin zone, corresponding to the M and R points. Through detailed analyses of the vibrational modes and bond strengths, we reveal that all four types of M atoms have softer bonding with neighboring Pu than Pu-Pu bond, which accounts for the phonon softening and may shed light on the δ -stabilization of Pu by trivalent metal doping. In addition, we find that, due to the missing p - d hybridization, Pu_3Al behaves quite differently from the other three Pu_3M compounds. For example, Pu_3Al has an unexpected equilibrium volume and high-frequency disentangled optical branches of phonons.

DOI: [10.1103/PhysRevB.100.184101](https://doi.org/10.1103/PhysRevB.100.184101)**I. INTRODUCTION**

Among all elements in the periodical table, plutonium (Pu) is probably the most fascinating one because of its vast mysterious properties [1–3]. It has the largest number of solid phases in all elemental metals, forming six allotropes between room temperature and the melting point. The most stable α phase has an unusual low-symmetry monoclinic structure and is as brittle as glass, which is quite different from normal metals. The high-symmetry δ phase is as malleable as normal metals, but has a negative thermal expansion coefficient, and so on. After a half-century of research, it is now widely accepted that these mysterious properties come from the complicated behaviors of the $5f$ electrons. First, Pu happens to stand in the middle site of the actinides, being the borderline between the light actinides with $5f$ electrons as itinerant as $5d$ electrons and the late actinides with localized $5f$ electrons resembling the $4f$ electrons. Second, the $7s$, $6d$, and $5f$ electrons of Pu have nearly equivalent energies, thus forming hybridized bands [1]. Until now, it was still challenging to explicitly explain the mechanisms of the unique properties of Pu. The difficulties lie both in experimental and theoretical sides. On the one hand, the high radioactivity of Pu makes it hard to handle in the laboratory. On the other hand, normal density functional theory (DFT) fails to correctly predict the structure and magnetic property of Pu at once, while dynamic mean-field theory (DMFT) requires too much computation to be applied for the systems containing tens of atoms [4]. Therefore, Pu still remains a puzzle in every aspect.

There has been some progress in understanding the unique magnetic property of Pu over the past decade. Kotliar *et al.* pointed out that the $5f$ electrons in δ -Pu show fluctuating valence states in 2007 [5], which has finally been experimentally confirmed through core-hole photoemission spectroscopy and resonant x-ray emission spectroscopy measurements in 2015 [6]. Then it is clear that the nonmagnetism in δ -Pu originates from the valence fluctuations of the $5f$ electronic states.

Besides nonmagnetism, another widely concerned mystery about δ -Pu is the stabilization after doping with other metals. δ -Pu adopts a face-centered cubic (fcc) structure and is the most favored phase in industrial applications. However, pure δ -Pu is only stable above 583 K. When alloyed with a small amount of certain metals, most of which are trivalent elements including Al, Ga, In, Sc, Tl, Am, and Ce, δ -Pu can be stabilized at room temperature and below [7,8]. However, pure δ -Pu has exotic negative thermal-expansion coefficients while δ -Pu with a light doping of Ga has normal thermal-expansion coefficients [9–11]. This puzzle has not even been touched at all.

Presently, the underlying mechanism of the δ -stabilization with IIIA or IIIB metal dopings has not been fully unraveled, but there have been quite a few attempts to figure out this issue. Robert *et al.* investigated the influence of the chemical short-range order on the phase diagrams of Pu-Al, Pu-Ga, and Pu-In alloys long ago [12–14]. Thereafter, mechanisms on the δ -stabilization were proposed including the Ga-strengthened orbital hybridizations [15,16], the varied correlation of the $5f$ electron [17], the altered stability of α -Pu, which, in turn, influences the phase transition [18–20], and so on. Recently, Dorado *et al.* calculated the phonon dispersion curves of δ -Pu in a 32-atom supercell and found that the imaginary branches exist, which is at odds with previous works [4].

*Corresponding author: yang_yu@iapcm.ac.cn

†Corresponding author: zhang_ping@iapcm.ac.cn

By doping one Ga atom into the Pu supercell, the imaginary bands are eliminated, which demonstrates the δ -stabilization by Ga-doping in a straightforward way.

Experimentalists reported the phonon dispersion curves for δ -Pu with a tiny addition of Ga and Al, in which a pronounced softening of the [111] mode was observed [21,22]. Via phonon calculations and bond strength analysis, Li *et al.* proposed that Pu_3Ga in the mixture of the alloys is responsible for the softening [23]. The studies on the phonon properties are thus significant and might provide an insight into the mechanism of δ -stabilization. However, Pu alloyed with other trivalent metals has not been thoroughly investigated on the phonon properties. Therefore, a systematical investigation of the Pu- M alloys is necessary, where M is a trivalent metal. Since Pu_3M compounds represent the Pu-rich side and have a relatively simple structure, we focus on Pu_3M in fcc structure (here M only represents the IIIA element including Al, Ga, In, and Tl) for the structural, electronic, and phonon properties. We find that the phonon branches for Pu_3M show remarkable softening at [011] and [111] zone boundaries. The soft modes both correspond to the relative motions between Pu atoms and the M - M atomic chains. We also demonstrate that the interaction between Pu and the M atom is softer than the interaction between Pu atoms, which accounts for the phonon softening in Pu_3M . However, due to the spin-orbit coupling and the nonzero magnetic moment, there is a slight tetragonal distortion in all the Pu_3M compounds and the tetragonality monotonously increases from Al to Tl. Moreover, Pu_3Al is found to be different from other three compounds in the lack of d electrons, therefore, the p - d hybridization in Pu_3Al is not as strong as in Pu_3Ga , Pu_3In , and Pu_3Tl , which is also the reason for the exceptionally large equilibrium volume of Pu_3Al .

II. COMPUTATIONAL DETAILS

All calculations are carried out in the frame work of density functional theory using the Vienna *ab initio* simulation package (VASP).[24,25] The projected augmented wave method is employed with an kinetic energy cutoff of 700 eV [26,27]. The Pu $5f$, $6s$, $6p$, $7s$; Al $3s$, $3p$; Ga $3d$, $4s$, $4p$; In $4d$, $5s$, $5p$; and Tl $5d$, $6s$, $6p$ electrons are included as valence electrons. The exchange and correlation interactions are treated in the generalized gradient approximation (GGA) using the Perdew-Burke-Ernzerhof (PBE) functional [28]. To describe the well-known correlated $5f$ orbitals, we adopt the GGA + U approach formulated by Dudarev *et al.* [29,30]. The effective U_{eff} , which is the difference between the Coulomb on-site U and exchange J parameters, is set as 4 eV, consistent with previous works [23,31]. Although the DFT + U method always yields a magnetic moment on Pu, which is not the fact in experiments on pure Pu metal, it can be good enough for the Pu- M compounds since the compounds are usually magnetic, such as Pu_3Ga which is antiferromagnetic according to the experiments [32]. Moreover, Amadon and Dorado showed that a simple GGA + U method can describe the structural properties of various phases of Pu as accurately as the combination of GGA with DMFT does [33]. Due to the relativistic effect on the heavy elements, we include the spin-orbital coupling (SOC) effect in the calculations

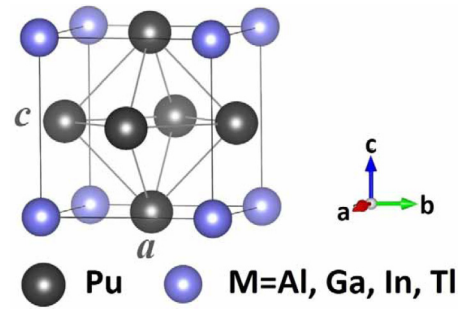


FIG. 1. The atomic structures of Pu_3M unit cell, where the c is a little larger than the a .

with the defaulted easy axis along the [001] direction, which inevitably specializes the [001] direction, breaks the cubic $Pm\bar{3}m$ ($Fm\bar{3}m$) symmetry and leads to the emerging of a new $P4/mmm$ symmetry. To optimize the structure, we first test the lattice dimensions by hand and find the values that minimize the energy. Then we set the initial lattice constants at these values and relax both the positions of the atoms and the lattice again until the net interatomic forces are smaller than 0.002 eV/Å. For the Pu_3M compounds, we construct the simplest $L1_2$ strukturbericht designation (AuCu_3 structure) which has the highest symmetry as shown in Fig. 1, where there are four atoms in a unit with the three Pu atoms occupying the face-centered positions and the M atom at the corner of the cubic [34]. The k -point grid of $11 \times 11 \times 11$ is employed for the relaxation of the unit cell, and k grids of $5 \times 5 \times 9$ and $5 \times 5 \times 5$ are employed for the total energy calculations of the 16-atom supercells and 32-atom supercells, respectively, which are used for the calculations of the phonon properties with the help of the PHONOPY package [35].

III. CRYSTAL STRUCTURE, ELECTRONIC STRUCTURE AND MAGNETIC PROPERTY OF Pu_3M

As pointed out by previous work [36–38], Pu_3Ga actually has two forms: one is the AuCu_3 -type structure at room temperature, denoted by $L1_2$ in the Strukturbericht designation, and the other is the SrPb_3 -type ($L6_0$) structure at low temperatures, which essentially is a slight tetragonal deformation of the $L1_2$ phase [39]. Also, in 1958, Bochvar *et al.* reported the experimental data of the tetragonal phase of Pu_3Al , giving a sizable tetragonality of 1.0087 [40]. Here we optimized the three lattice dimensions as well as the atomic positions for Pu_3M starting from the initial cubic structure, and found that all four compounds indeed relax to the tetragonal structures. The calculated lattice dimensions as well as the experimental values are shown in Table I, in which the experimental lattice parameter a of Pu_3In and Pu_3Tl are for the cubic phase due to a lack of available data for their tetragonal phase. The difference between theoretical results and experimental results lies within the limitation of the GGA + U method. Although the calculated tetragonality, i.e., the c/a ratio, of each Pu_3M is quite near unity as shown in Table I, the tetragonal distortion is robust under different initial settings. Interestingly, the tetragonality increases monotonically with the atomic number of M . This trend is in agreement with the trend of the magnetic

TABLE I. The lattice dimensions (calculated in this work and from previous experiments), tetragonality (c/a ratio), equilibrium volume per atom, and magnetic moment on each Pu atom which includes the spin moment and the orbital moment for the Pu_3M compounds.

	Lattice dimensions (\AA)				Tetrago- nality	Volume per atom (\AA^3)	Magnetic moment per Pu (μ_B)			
	Theor.		Exp.				Spin	Orbital	Total	Exp.
	a	c	a	c						
Pu_3Al	4.668	4.693	4.499 ^a	4.538 ^a	1.00536	25.56	5.30	-3.46	1.84	
Pu_3Ga	4.653	4.679	4.469 ^b	4.527 ^b	1.00559	25.32	5.30	-3.46	1.84	0.88 ^c
Pu_3In	4.809	4.836	4.702 ^d		1.00561	27.96	5.34	-3.46	1.88	
Pu_3Tl	4.824	4.858	4.723 ^d		1.00705	28.26	5.38	-3.47	1.92	

^aFrom Ref. [40].

^bFrom Ref. [38].

^cFrom Ref. [32].

^dFrom Ref. [41].

moment shown in Table I. Taking the SOC effect into account in the spin-polarized calculations, we find that the total magnetic moment of each Pu atom is nonzero and orients along the [001] direction. Such a magnetic orientation distinguishes the c -axis from the in-plane $a(b)$ -axis, and breaks the cubic symmetry. The spin moment increases from Pu_3Al to Pu_3Tl while the orbital moment remains nearly unchanged, thus the total magnetization increases. On the one hand, the increasing net magnetization leads to the enhanced discrepancy between the c -axis and the in-plane axes. On the other hand, the heavier element means stronger relativistic effect and worse symmetry breaking. Therefore, the tetragonality rises from Pu_3Al to Pu_3Tl .

In addition, the spin moment of the Pu atom is about 5.3 to $5.4 \mu_B$, which only differs slightly from Pu_3Al to Pu_3Tl , consistent with the $5f^6$ configuration of Pu. Owing to the orbital moment, the large spin moment is partly canceled and the net magnetization is about 1.8 to $1.9 \mu_B$ per Pu. Although the Pu metal shows no magnetization in experiments, Pu_3Ga is proven to be magnetic with a Néel temperature of 40.3 K [32]. Our results thus do not conflict with experimental work. Unfortunately, the calculated total magnetic moment is still much larger than the experimental value of $0.88 \mu_B$ for Pu_3Ga [32].

In Table I, the lattice dimensions and equilibrium volumes for Pu_3M are listed, which are slightly larger than the experimental values due to the well-known GGA overestimation [42,43]. One can see that except for Al, other Pu_3M compounds go through volume expansions when increasing the atomic radii of the M atom. As we will discuss in the following, the unexpected large cell volume of Pu_3Al comes from the different bonding character of Pu-Al compared to other Pu- M bondings.

Figure 2 shows the projected density of states (PDOS) on Pu d , Pu f , and $M p$ orbitals for the four Pu_3M compounds since these states contribute most to the energy range around the Fermi level. As shown, the Pu f states always locate above the Fermi level and 2 eV below the Fermi level for all Pu_3M compounds; while the d states of the Pu atom and p states of the M atom distribute mostly from 2 eV below the Fermi energy. Nevertheless, the electronic hybridizations in this energy interval show different characters for different compounds. For Pu_3Ga , Pu_3In , and Pu_3Tl , the Pu- d , and M - p electronic states seem to hybridize effectively judging

from their considerable distributions. In contrast, the Al- p state is almost missing from 2 eV below the Fermi energy in the PDOS of Pu_3Al , implying that there exists very weak electronic hybridization between Pu and Al atoms.

Moreover, we calculated the band characterizations for M atoms in the four Pu_3M compounds around the Fermi level as shown in Fig. 3. The decomposed weights of M atoms are

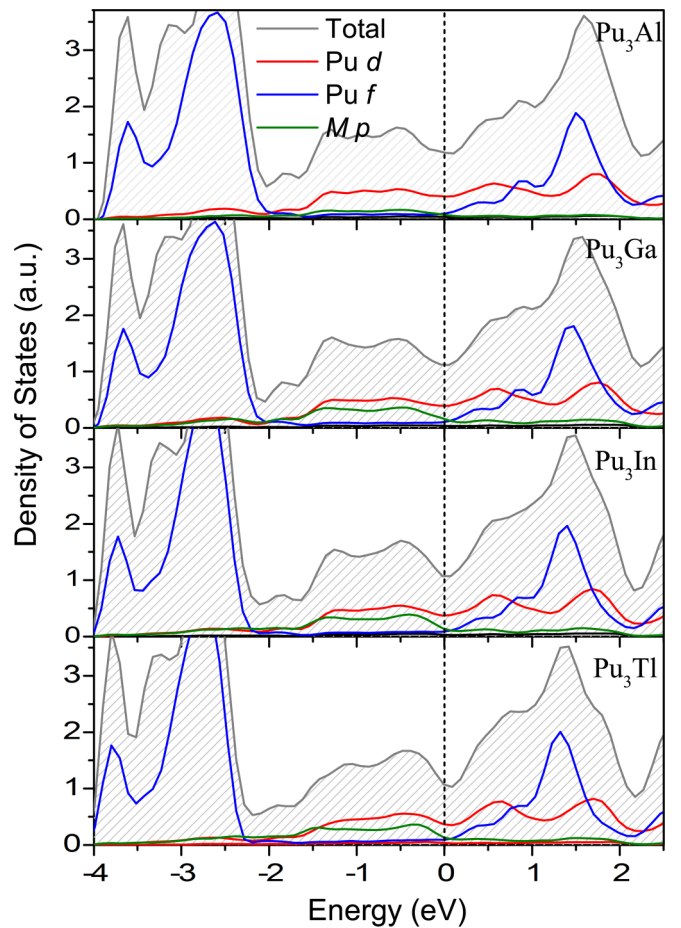


FIG. 2. The total densities of states (TDOS) and projected densities of states (PDOS) on Pu f , Pu d , and $M p$ orbitals in Pu_3M compounds. As a guide for the eyes, the total densities of states are divided by 3.

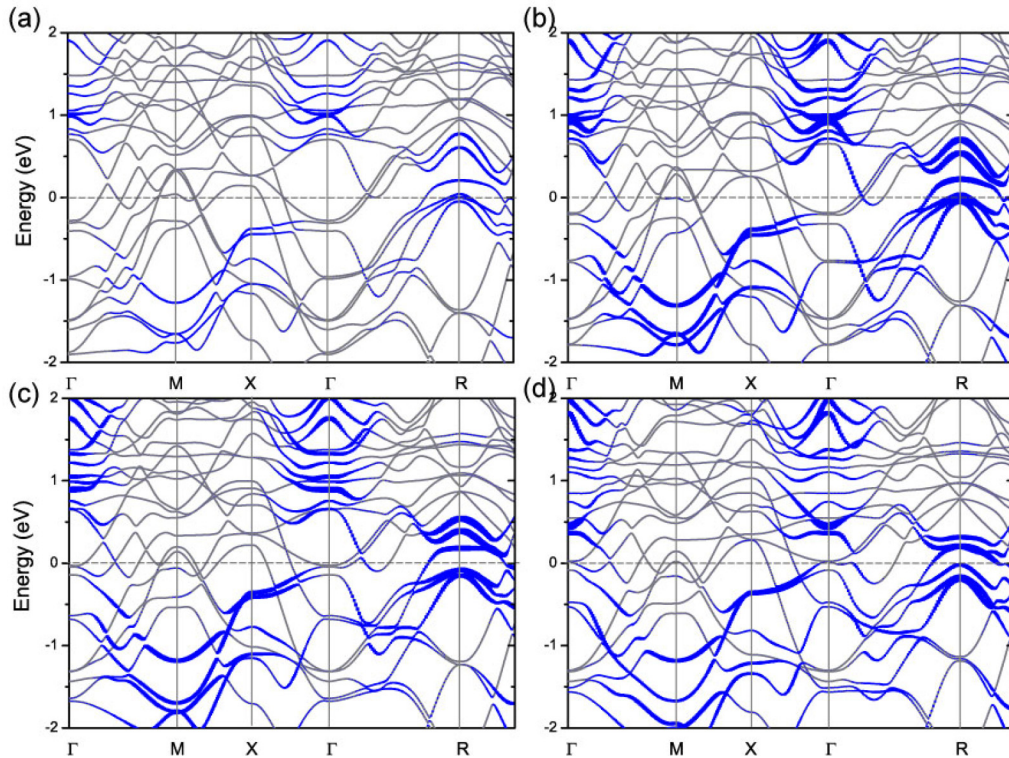


FIG. 3. Calculated band structures of (a) Pu_3Al , (b) Pu_3Ga , (c) Pu_3In , and (d) Pu_3Tl with the resolved components from M atoms. The thickness of the blue ribbons indicates the contribution from the M atom to the parent bands. The Fermi level is set to zero.

indicated by the thickness of the blue ribbons. Comparing Pu_3Al to the other three compounds, one can find that the contributions from Al atom to the Pu_3Al bands are much smaller than that of other M atoms to their parent bands. Therefore, the atom-decomposed band structure is another proof for the weak hybridization between Al and Pu in Pu_3Al , which probably leads to the unexpectedly larger equilibrium volume of Pu_3Al in comparison to Pu_3Ga .

Some previous works regarded the electronegativity difference as a dimension to determine the formation heat and charge transfer in binary alloys or compounds [44,45]. The electronegativity values of Al, Ga, In, and Tl are 1.61, 1.81, 1.78, and 1.62 in the Pauling scale, respectively, all of which are larger than the electronegativity of Pu (1.28), meaning that electrons tend to transfer from Pu to M [46,47]. Generally the electronegativity decreases when moving down the periodic table since the screening by the inner electrons increases, however, the electronegativity of Al is weaker than that of the other three M metals. As a result, the particularity for Pu_3Al in electronegativity difference emerges, in accord with the particularity for Pu_3Al in electronic hybridizations and equilibrium volumes of Pu_3M compounds.

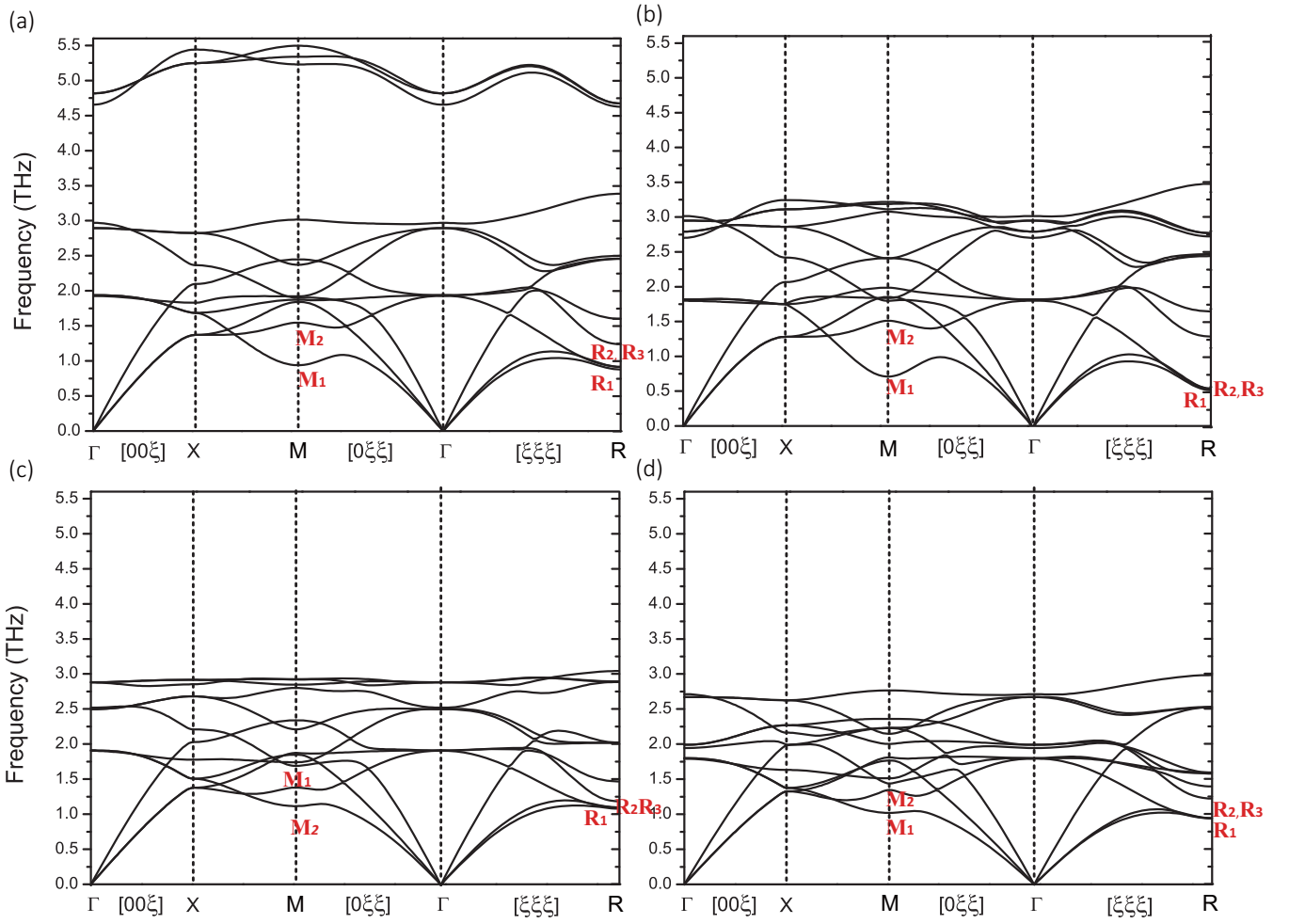
IV. PHONON SPECTRA AND VIBRATIONAL MODES

The phonon dispersion curves for the four Pu_3M compounds were calculated using the finite-displacement method in combination with DFT + U [48], which has been demonstrated to be reasonable enough when applied to the phonon properties of Pu_3Ga [23]. The smallest unit cell of Pu_3M has four atoms, while $\delta\text{-Pu}$ has a single-atom unit cell. To make

effective comparisons, we then project the phonon dispersion curves of $\delta\text{-Pu}$ along the high-symmetry lines of the Brillouin zone of the four-atom cubic cell of $\delta\text{-Pu}$. In such a way, the R point with the fractional reciprocal coordinate of $(1/2, 1/2, 1/2)$ of the four-atom cubic cell corresponds exactly to the L point in the first Brillouin zone of one-atom unit cell of $\delta\text{-Pu}$. Thus we can make comparisons and investigate the influences of the M doping on the phonon softening at the L point in $\delta\text{-Pu}$ [21,22,49,50].

Generally, the phonon frequencies decrease from Pu_3Al to Pu_3Tl as shown in Fig. 4, as the atomic masses of M increase. Again, the phonon dispersion curves of Pu_3Al are different from those of other compounds by the impressively decoupled high-energy phonon branches as shown in Fig. 4(a). The three highest phonon modes in the range of 4.5 to 5.5 THz are the sole displacements of Al ions, which we identified, and are well separated from other phonons by more than 1.3 THz. This feature is additional evidence for the weak bonding between Pu and Al atoms, and further accounts for the abnormally large equilibrium volume of Pu_3Al . In contrast, in Pu_3Tl all the phonons are entangled, of which the frequencies are all smaller than 3 THz, because the atomic mass of Tl is closer to the mass of Pu. The phonons of Pu_3Ga and Pu_3In have higher energies than those of Pu_3Tl , but are all coupled together notably, which suggests highly involved vibrations of the Pu and Ga/In atom.

In our previous work [23], we pointed out that there was a significant phonon softening in the transverse acoustic branch at the L point in the Brillouin zone of Pu_3Ga , in comparison to $\delta\text{-Pu}$. That finding to some extent explains the earlier reported experimental result [22]. Here in the present study, we find

FIG. 4. Phonon dispersion curves for (a) Pu₃Al, (b) Pu₃Ga, (c) Pu₃In, and (d) Pu₃Tl.

that the phonon softening in the transverse acoustic branch at the R (L) point is a common feature for Pu₃Al, Pu₃Ga, Pu₃In, and Pu₃Tl. In addition, we find that the transverse branches also undergo phonon softening at the M point, as shown in Fig. 4.

For all the four Pu₃M compounds, the lowest transverse modes at the M point are nondegenerate, denoted by M₁ as shown in Fig. 4, whereas the second lowest phonon mode marked as M₂ does not have softening at the M point and is observably separated from M₁. The lowest-frequency modes at the R point have similar frequencies. Table II lists the phonon frequencies at the zone boundary points, i.e.,

TABLE II. The vibrational frequencies of M₁, M₂, R₁, R₂, and R₃ modes of Pu₃M. All values are in units of THz.

	Frequency				
	M ₁	M ₂	R ₁	R ₂	R ₃
δ-Pu	1.3691		1.3978		
Pu ₃ Al	0.9390	1.5461	0.8777	0.9149	0.9149
Pu ₃ Ga	0.7090	1.5110	0.5151	0.5381	0.5381
Pu ₃ In	1.1146	1.3795	1.0786	1.0957	1.0957
Pu ₃ Tl	1.0189	1.3457	0.9419	0.9431	0.9431

M = (0, 1/2, 1/2)π/a and R = (1/2, 1/2, 1/2)π/a points, in comparison to the phonon frequencies of δ-Pu at the same points. One can see that the lowest mode at the R point (R₁ mode) is nondegenerate while the other two vibrational modes are two-fold degenerate and denoted by R₂ and R₃, respectively.

Since the phonon softening at M and R is a common feature for all the Pu₃M (M = Al, Ga, In, Tl) compounds, and differentiates these compounds from δ-Pu, one would naturally think that the stabilization of δ-Pu through alloying with these four elements might have certain connections with the corresponding vibrational properties. Therefore, we next analyze the vibrational modes for the transverse phonon branches at M and R. To reproduce the [011] modes at the zone boundary, i.e., the M point, a doubling of the original unit cell along the [011] direction is required; by the same token, the [111] modes at zone boundary denoted by R need a doubled cell along the [111] direction. We find that the vibrational modes are the same for all the four Pu₃M compounds, and we will not specify the M element in the following discussions. Figure 5 shows the atomic displacements in the above phonon modes at M and R points in the further enlarged supercells. The two lowest modes at the M point, as demonstrated in Figs. 5(a) and 5(b), are alike and at the same time delicately different. As seen

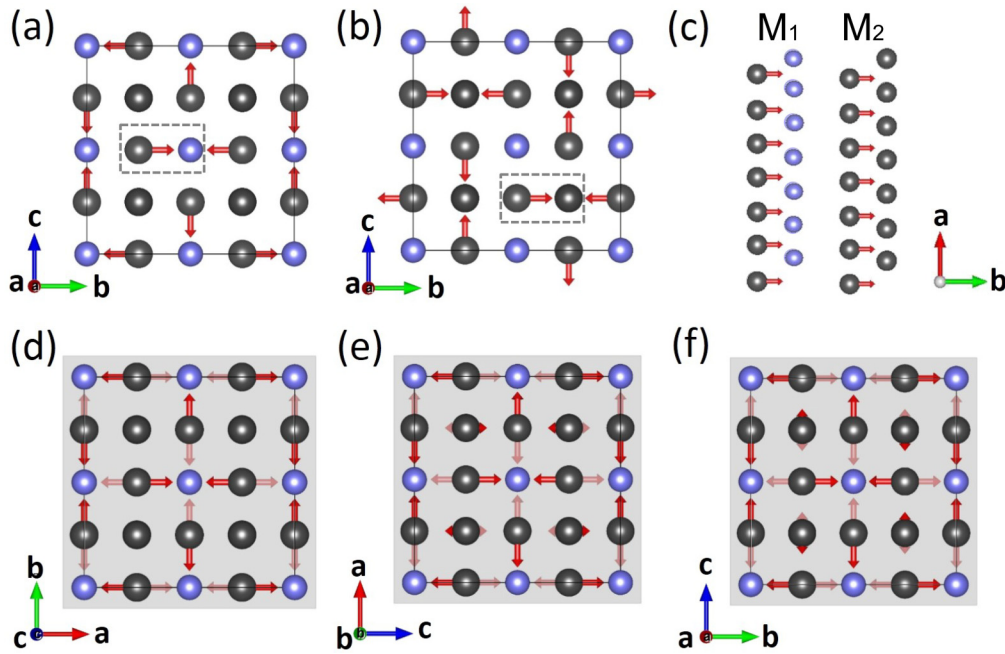


FIG. 5. The atomic displacements of different vibrational modes of the Pu_3M compounds: (a) M_1 mode; (b) M_2 mode; (d) R_1 mode; (e) R_2 mode; and (f) R_3 mode. To clarify the difference between M_1 and M_2 modes, side views of the local atomic displacements in the dashed rectangles of the M_1 and M_2 modes are also shown in (c). The Pu (M) ions are represented with dark grey (blue) spheres and the atomic displacements are represented with red arrows which are roughly proportional to the magnitudes of the displacements. For the M point, the unit cell is enlarged by 2×2 in the bc plane. While for the R point, the unit cell is doubled in the three dimensions. Therefore, translucent planes are put between two layers of the unit cells parallel to the plane, and the bright red arrows are the displacements of the ions in the first layer and the shadowed red arrows are for the second layer. Note that the seemingly neighbored atoms actually are not in the same plane (due to the limitation of the plane graph). They have an offset of $1/2$ along the normal axis, as shown in the side view of (c).

in the figures, the M_1 mode consists of the rotation of the Pu atoms around a central Pu atomic chain, and the M_2 mode is the rotation of the Pu atoms around the M atomic chain. The two modes would be degenerate if it were not for the substitution of M atoms. (Actually these two branches indeed intersect at the M point in δ -Pu [23].) Specifically, as shown in the side view of Fig. 5(c), Pu atoms move toward the M atomic chains in the M_1 mode, resulting in the shortening of half of the Pu- M bonds and stretching of the other half of the Pu- M bonds. While in the M_2 mode, the Pu displacements point to the Pu-Pu chain, which is nearly unrelated to the Pu- M bonds.

Comparatively, the R_1 , R_2 , and R_3 vibrational modes are more complicated. As shown in Fig. 5(d), the R_1 mode is the rotation around a central Pu atomic chain, which is similar to the M_1 mode only that the rotational axis is along c -axis and the two successive rotations are antiphase. The R_2 mode and R_3 mode are degenerate and of slightly higher energy than the R_1 mode. They are the rotations around the Pu atomic chains along the b -axis and a -axis, respectively. But the Pu atoms of the central Pu-Pu chain are not static, instead, they have small oscillations of which the displacements are one magnitude smaller than those of the rotating Pu atoms, as shown in Figs. 5(e) and 5(f). Besides, in R_2 and R_3 modes, the displacements of the surrounding Pu atoms are not completely in the plane normal to the central Pu atomic chain. In other words, the rotations of the Pu atoms are slightly canted towards the rotational axis [which could not be shown in Figs. 5(e) and 5(f) for the limitation of two-dimensional graph]. Although the

canting of the rotation together with the small oscillations of the central Pu attributes to the elevation of the R_2/R_3 mode, R_1 , R_2 , and R_3 modes have a main character in common, that is the Pu- M chemical bonding dominates the vibration as in the M_1 mode.

In total, we can see that all the softening vibrational modes have their connections with the Pu- M bonds. In δ -Pu, there are no such Pu- M bonds and thus no phonon softening exists. Normally, the lowering down in vibrational frequency corresponds to the weakening in bonding strength. Therefore, the phonon softening indicates that all Pu- M bonds are somehow softer than Pu-Pu bonds. We then draw the phonon energy curves for atomic displacements along each vibrational modes. As shown in Fig. 6(a), the energy increases with the increasing of the atomic displacements. Obviously, displacements in the M_1 mode cause less energy growing than those in the M_2 mode for each Pu_3M compound. Meanwhile, the energy increasing caused by the M_2 mode is at the same level with that caused by the [011] mode in pure δ -Pu, which is not surprising since they are both dominated by the Pu-Pu interaction. In conclusion, the lower energies of the M_1 modes relative to the M_2 mode in Pu_3M and [011] mode in δ -Pu prove that Pu- M bonds are softer than Pu-Pu bonds. And Pu atoms move more freely towards the M atoms than towards Pu atoms. Similarly to the M_1 and M_2 modes, we also plot the phonon energy in the supercell which reproduces the R_1 mode versus the atomic displacements for Pu_3M in comparison to the same-size supercell of δ -Pu reproducing the [111] mode (i.e., the L mode). As shown in Fig. 6(b), the energy increasing

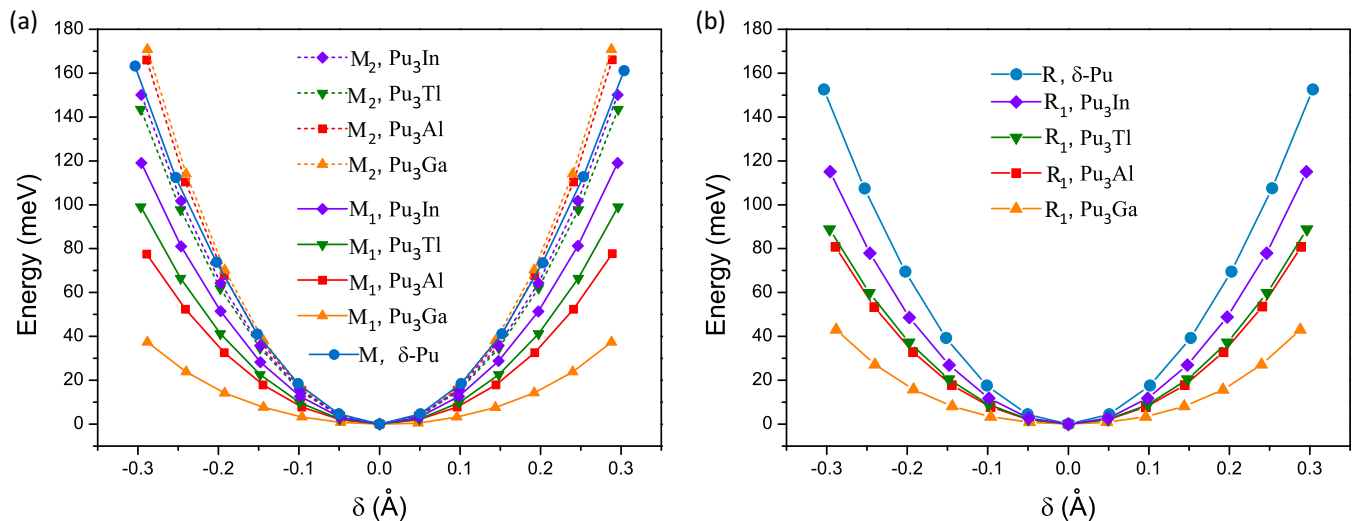


FIG. 6. Energies of the Pu_3M and $\delta\text{-Pu}$ with different atomic displacements of the investigated phonon modes: (a) M_1 , M_2 modes in Pu_3M and $[011]$ mode in $\delta\text{-Pu}$; (b) R_1 mode in Pu_3M and $[111]$ mode in $\delta\text{-Pu}$. Note that the calculations are performed in the enlarged supercells, but the energies are averaged on the formula unit of Pu_3M (in the $\delta\text{-Pu}$ case the energies are for the 4-atom conventional cell).

induced by the R_1 mode in Pu_3M compounds are all smaller than that of the $[111]$ mode in $\delta\text{-Pu}$. The energy curves for the R_2 and R_3 modes are just similar and thus are not shown. So the phonon softening of Pu_3M at both M and R points all comes from the softer Pu-M bonds. The softer

bonds allow Pu atoms to drift more freely in Pu_3M than in $\delta\text{-Pu}$.

In the above vibrational modes, the displacements of M atoms are tiny. By manually moving the M atom towards its 12 nearest neighbors as shown in Fig. 7(a) and calculating the

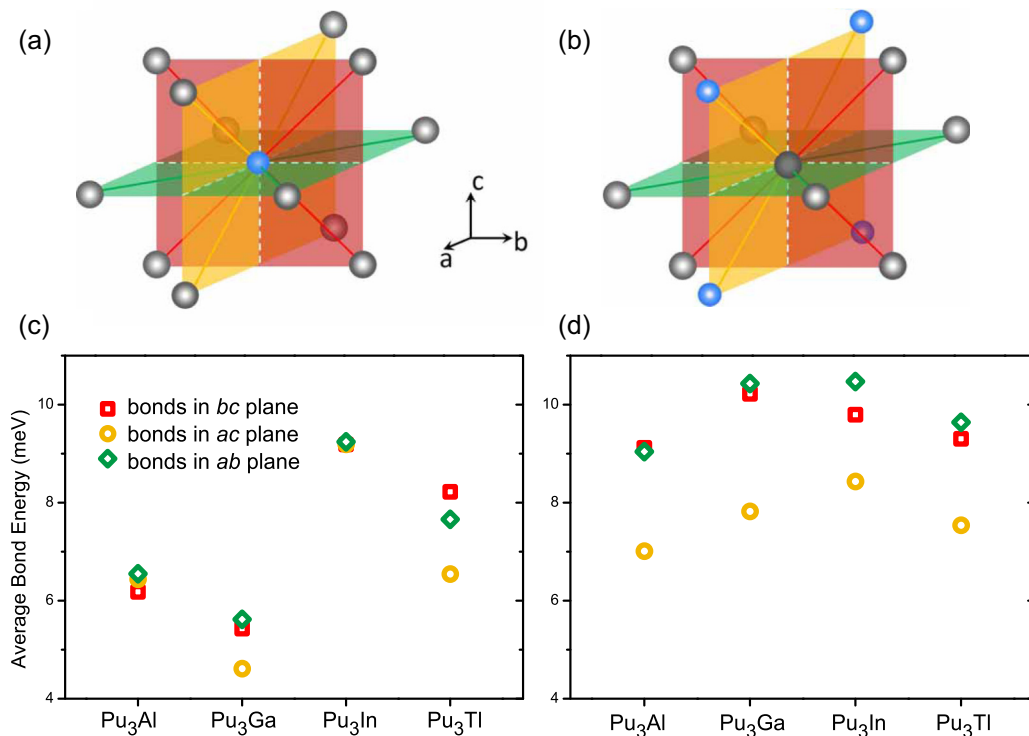


FIG. 7. Schematic plots of (a) a central M atom and its 12 nearest neighbors and (b) a central Pu atom and its 12 nearest neighbors in a Pu_3M supercell. The big grey spheres (small blue spheres) represent Pu (M) atoms. The red, yellow, and green planes represent the orthogonal bc , ac , and ab planes, respectively. The colored lines on the transparent planes denote the bonds between central atoms and the nearest neighbors. The white dashed lines are only guides to the eyes. The bond strength is quantitatively represented by the energy difference between the undistorted supercell and the supercell with the central atom moving along the corresponding bond direction by 2%. By this method, the average bond strengths in bc , ac , and ab planes for Pu_3M are calculated and shown in (c) and (d) in units of meV. Here (c) corresponds to the case of (a) where the central M atoms are displaced towards the nearest neighbors and (d) corresponds to (b) by the same token.

change of the energy, we estimate the bond strength and bond anisotropy of M with the adjacent Pu atoms. The average bond strengths in three orthogonal planes are plotted in Fig. 7(c) for M -Pu bonds in Pu_3M , and Ga has the smallest bond strengths with its neighbors in consistence with Fig. 6. For comparison, the bond strengths of a Pu atom with surrounding atoms in Pu_3M are also investigated in the same way and shown in Figs. 7(b) and 7(d). Overall, the average bond strengths of Pu and its neighbors are larger. It is interesting that the average bond strength in the plane on which M atoms are located is remarkably smaller than the average bond strengths in the other two planes. This result further corroborates that Pu atoms tend to move towards the neighboring M atoms and the bond between Pu and M atoms is softer than the Pu-Pu bond.

V. CONCLUSION

We systematically investigate the structural, electronic, and phonon properties of the Pu_3M compounds, where $M = \text{Al}$, Ga, In, and Tl, using density functional theory calculations plus U with spin-orbit coupling effect taken into account. The optimized Pu_3M structures have a slight tetragonal distortion from the fcc structure, in good agreement with previous works. The equilibrium volumes of Pu_3M increase with the increase of the atomic number of M , except for Pu_3Al , which is attributed to the poor p - d hybridization strength between Pu and Al compared to that between Pu and other M atoms reflected by the projected density of states and decomposed band structures with M contributions. Importantly, we find that the phonon dispersion curves of all the Pu_3M compounds ($M = \text{Al}$, Ga, In, Tl) show phonon softening at the M and

R points in the reciprocal space. By carefully analyzing the atomic displacements of the vibrational modes, we find that both the lowest modes at the R and M points are the rotations of Pu atoms around a central Pu-Pu atomic chain. In these vibrational modes, the distances between Pu atoms and the M atomic chain change periodically while the Pu-Pu distances are nearly unchanged, hence the Pu- M interactions dominate the phonon softening at these points. The calculated phonon energies of the supercells with the reproduced phonon modes at M and R points as functions of the atomic displacements, as well as the calculated nearest-neighboring bond strengths, verify that all the Pu- M bonds are softer than the Pu-Pu bonds, which is the crucial reason for the anomalous phonon behaviors. Our work might provide some clues on the δ -stabilization of Pu alloys.

ACKNOWLEDGMENTS

The computer simulations were carried out on the high performance computing facility from the NSCC-GZ National Supercomputing Center and Lvliang Cloud Computing Center. This work was supported by the Science Challenge Project under Grant No. TZ2018004, by the National Natural Science Foundation of China under Grant No. 11704038, Grant No. 11625415, and Grant No. 11974055, by the Joint Fund of the National Natural Science Foundation of China and the China Academy of Engineering Physics (NSFC-NSAF) under Grant No. U1530258 and Grant No. U1630248, by the Open Research Fund Program of the State Key Laboratory of Low-Dimensional Quantum Physics under Grant No. KF201712, and by the Research Fund Program of the Key Laboratory of Computational Physics.

-
- [1] S. Hecker, *Metall. Mater. Trans. A* **35**, 2207 (2004).
 [2] S. S. Hecker, *Los Alamos Sci.* **26**, 290 (2000).
 [3] K. T. Moore and G. van der Laan, *Rev. Mod. Phys.* **81**, 235 (2009).
 [4] B. Dorado, J. Bieder, and M. Torrent, *J. Phys.: Condens. Matter* **29**, 245402 (2017).
 [5] J. H. Shim, K. Haule, and G. Kotliar, *Nature* **446**, 513 (2007).
 [6] M. Janoschek, P. Das, B. Chakrabarti, D. L. Abernathy, M. D. Lumsden, J. M. Lawrence, J. D. Thompson, G. H. Lander, J. N. Mitchell, S. Richmond, M. Ramos, F. Trouw, J. X. Zhu, K. Haule, G. Kotliar, and E. D. Bauer, *Sci. Adv.* **1**, e1500188 (2015).
 [7] F. H. Ellinger, W. N. Miner, D. R. O'Boyle, and F. W. Schonfeld, *Constitution of Plutonium Alloys* (Dec.), Los Alamos National Laboratory report LA-3870-MS (1968).
 [8] S. S. Hecker, D. R. Harbura, and T. G. Zocco, *Prog. Mater. Sci.* **49**, 429 (2004).
 [9] F. H. Ellinger, *Trans. Am. Inst. Min. Metall. Pet. Eng.* **206**, 1256 (1956).
 [10] T. Sandenaw, *J. Phys. Chem. Solids* **16**, 329 (1960).
 [11] J. M. Taylor, *J. Nucl. Mater.* **31**, 339 (1969).
 [12] G. Robert, C. Colinet, B. Siberchicot, and A. Pasturel, *Modelling Simul. Mater. Sci. Eng.* **12**, 693 (2004).
 [13] G. Robert, A. Pasturel, and B. Siberchicot, *Phys. Rev. B* **68**, 075109 (2003).
 [14] G. Robert, A. Pasturel, and B. Siberchicot, *J. Phys.: Condens. Matter* **15**, 8377 (2003).
 [15] S. C. Hernandez, D. S. Schwartz, C. D. Taylor, and A. K. Ray, *J. Phys.: Condens. Matter* **26**, 235502 (2014).
 [16] P. Söderlind, A. Landa, J. E. Klepeis, Y. Suzuki, and A. Migliori, *Phys. Rev. B* **81**, 224110 (2010).
 [17] L. Havela, A. Shick, and T. Gouder, *J. Appl. Phys.* **105**, 07E130 (2009).
 [18] J.-X. Zhu, R. C. Albers, K. Haule, G. Kotliar, and J. M. Wills, *Nat. Commun.* **4**, 2644 (2013).
 [19] B. Sadigh and W. G. Wolfer, *Phys. Rev. B* **72**, 205122 (2005).
 [20] G. Robert, P. Legrand, and S. Bernard, *IOP Conf. Series: Mater. Sci. Eng.* **9**, 012085 (2010).
 [21] R. J. McQueeney, A. C. Lawson, A. Migliori, T. M. Kelley, B. Fultz, M. Ramos, B. Martinez, J. C. Lashley, and S. C. Vogel, *Phys. Rev. Lett.* **92**, 146401 (2004).
 [22] J. Wong, M. Krisch, D. L. Farber, F. Occelli, A. J. Schwartz, T.-C. Chiang, M. Wall, C. Boro, and R. Xu, *Science* **301**, 1078 (2003).
 [23] M. Li, Y. Yang, F. Zheng, and P. Zhang, *Phys. Rev. B* **96**, 134102 (2017).
 [24] G. Kresse and J. Furthmüller, *Phys. Rev. B* **54**, 11169 (1996).
 [25] G. Kresse and J. Furthmüller, *Comput. Mater. Sci.* **6**, 15 (1996).

- [26] P. E. Blöchl, *Phys. Rev. B* **50**, 17953 (1994).
- [27] G. Kresse and D. Joubert, *Phys. Rev. B* **59**, 1758 (1999).
- [28] J. P. Perdew, K. Burke, and M. Ernzerhof, *Phys. Rev. Lett.* **77**, 3865 (1996).
- [29] S. L. Dudarev, G. A. Botton, S. Y. Savrasov, C. J. Humphreys, and A. P. Sutton, *Phys. Rev. B* **57**, 1505 (1998).
- [30] S. L. Dudarev, D. N. Manh, and A. P. Sutton, *Philos. Mag. B* **75**, 613 (1997).
- [31] Y. Lu, Y. Yang, and P. Zhang, *Journal of Alloys and Compounds* **649**, 544 (2015).
- [32] V. E. Arkhipov, F. A. Kassan-Ogly, A. V. Korolev, S. V. Verkhovskii, Yu. N. Zuev, and I. L. Svyatov, *J. Nucl. Mater.* **385**, 42 (2009).
- [33] B. Amadon and B. Dorado, *J. Phys.: Condens. Matter* **30**, 405603 (2018).
- [34] W. B. Pearson, *The Crystal Chemistry and Physics of Metals and Alloys* (Wiley-Interscience, New York, 1972), p. 322.
- [35] A. Togo, F. Oba, and I. Tanaka, *Phys. Rev. B* **78**, 134106 (2008).
- [36] P. Söderlind and A. Landa, *J. Nucl. Mater.* **448**, 310 (2014).
- [37] G. Robert, C. Colinet, B. Siberchicot, and A. Pasturel, *Philos. Mag.* **84**, 1877 (2004).
- [38] F. H. Ellinger, C. C. Land, and V. O. Struebing, *J. Nucl. Mater.* **12**, 226 (1964).
- [39] P. Villars, and K. Cenzual, *Structure Types. Part 11: Space Groups (135) P4₂/mbc·C(123) P4/mmm* (Springer, Berlin, 2012).
- [40] A. A. Bochvar, S. T. Konobeevsky, V. I. Kutaitsev, T. S. Minshikova, and N. T. Chebotarev, *Soviet J. At. Energy* **15**, 1177 (1958).
- [41] O. J. Wick, *Plutonium Handbook A Guide to the Technology* (Gordon and Breach, New York, 1967).
- [42] M. E. Kassner and D. E. Peterson, *Bull. Alloy Phase Diagrams* **2**, 1843 (1990).
- [43] P. Villars and L. D. Calvert, *Pearson's Handbook of Crystallographic Data for Intermetallic Phases* (Materials Park, OH: American Society for Metals) **78**, 134106 (1985).
- [44] T. S. Chou, M. L. Perlman, and R. E. Watson, *Phys. Rev. B* **14**, 3248 (1976).
- [45] D. V. Louzguine-Luzgina and A. Inoue, *Appl. Phys. Lett.* **88**, 011911 (2006).
- [46] L. Pauling, *J. Am. Chem. Soc.* **54**, 3570 (1932).
- [47] A. L. Allred, *J. Inorg. Nucl. Chem.* **17**, 215 (1961).
- [48] K. Parlinski, Z. Q. Li, and Y. Kawazoe, *Phys. Rev. Lett.* **78**, 4063 (1997).
- [49] X. Dai, S. Y. Savrasov, G. Kotliar, A. Migliori, H. Ledbetter, and E. Abrahams, *Science* **300**, 953 (2003).
- [50] P. Söderlind, F. Zhou, A. Landa, and J. E. Klepeis, *Sci. Rep.* **5**, 15958 (2015).